1986

Simple Models for Diaphragm-Type Chlorine/Caustic Cells II. Effect of Acidic Anolyte on Steady-State Caustic Yield

John Van Zee
University of South Carolina - Columbia, vanzee@engr.sc.edu

Ralph E. White
University of South Carolina - Columbia, white@cec.sc.edu

Publication Info

Journal of the Electrochemical Society, 1986, pages 508-515.

Publisher's Version: http://dx.doi.org/10.1149/1.2108610
DOI: 10.1149/1.2108610

Simple Models for Diaphragm-Type Chlorine/Caustic Cells

II. Effect of Acidic Anolyte on Steady-State Caustic Yield

John Van Zee*

Department of Chemical Engineering, University of South Carolina, Columbia, South Carolina 29208

R. E. White*

Department of Chemical Engineering, Texas A&M University, College Station, Texas 77843

ABSTRACT

A simple steady-state model of a diaphragm-type chlorine/caustic cell in which the diaphragm is divided into two regions by a homogeneous acid-base reaction is presented. The location of the reaction affects significantly the caustic yield and effluent concentration. The model is used to predict the location of this reaction as a function of the operating variables, the physical constants, and three measurable properties of the diaphragm. These measurable properties are the MacMullin number or resistivity ratio of electrolyte-filled diaphragm relative to the electrolyte, the Darcy's law diaphragm permeability, and the diaphragm thickness. The model is used to predict a maximum in the relationship between the caustic yield and caustic effluent concentration. The model predictions are compared with experimental data by using parameter estimation techniques to determine the diffusion coefficients of hydroxyl and hydrogen ions and the average specific conductivity of the electrolyte within the diaphragm during operation of the cell.

In some industrial chlorine/caustic cells, the anolyte is acidic even though the feed brine is neutral or slightly basic because the dissolved chlorine hydrolyzes according to the following homogeneous reaction (1)

$$Cl_{2(aq)} + H_2O \rightleftarrows HOCl + H^+ + Cl^- \quad [1]$$

(See Ref. (1) for a discussion of the anolyte chemistry.) In other industrial cells, the anolyte may be acidic because HCl is fed to the cell to minimize the electrochemical formation of oxygen and to obtain as much gaseous chlorine as possible according to the equilibrium of reaction [1]. It is possible, then, that the acid/base neutralization reaction

$$OH^- + H^+ \rightarrow H_2O \quad [2]$$

occurs somewhere within the diaphragm. In this event, reaction [2] would contribute to the loss of catholyte OH^- ions, as well as to the losses due to the diffusion and migration of OH^- described in the previous paper (2). In addition, the existence of H^+ ions in the diaphragm could cause degradation of an asbestos diaphragm (1).

It is desirable, therefore, to have a simple[1] mathematical model to predict the steady-state effect that reaction [2] would have on the caustic yield and to predict the extent to which H^+ ions exist within the diaphragm. It is also desirable to base the model on measurable diaphragm properties so that model predictions could be compared to industrial and experimental cells. The model presented here includes the measurable diaphragm properties (3) that were used in our previous papers on simple steady-state models (4, 5). The effect of H^+ ions is included in this model by assuming that reaction [2] occurs at a plane within the diaphragm, the location of which depends on the operating conditions of the cell (*i.e.*, current density, differential head, anolyte *p*H, and temperature), the transport parameters, and the diaphragm properties. Thus, the model can be used to predict the operating conditions and diaphragm properties that would result in a reaction plane located at the anolyte/diaphragm interface, which has been claimed to be optimal for some practical cells (6). After the model is presented, it will be discussed in terms of dimensionless groups and then compared to experimental data to obtain pertinent transport parameters by nonlinear regression.

Model

The model is developed by considering Fig. 1 and using the well-known chemical engineering concept of a reaction plane (see Ref. (7), *e.g.*, for a general discussion, and Ref. (8, 9) for an example of an application in electrochemical systems). The model consists of assumptions and equations.

The assumptions of the model are: (*i*) dilute solution theory applies (10); (*ii*) only the spatial coordinate perpendicular to the diaphragm (*i.e.*, through the diaphragm from the anolyte to the catholyte) is important; (*iii*) the diaphragm properties (N_M, t, and P) are constant with time; (*iv*) the effective diffusion coefficients in the porous diaphragm can be written as a ratio of the free-stream diffusion coefficients to the MacMullin number (11)

$$D_{i,e} = D_i\epsilon/\tau = D_i/N_M \quad [3]$$

(*v*) the current density through the diaphragm is simply related to the potential gradient through the diaphragm by an effective average specific conductivity (4)

$$i = \frac{-\kappa}{N_M}\frac{d\Phi}{dx} \quad [4]$$

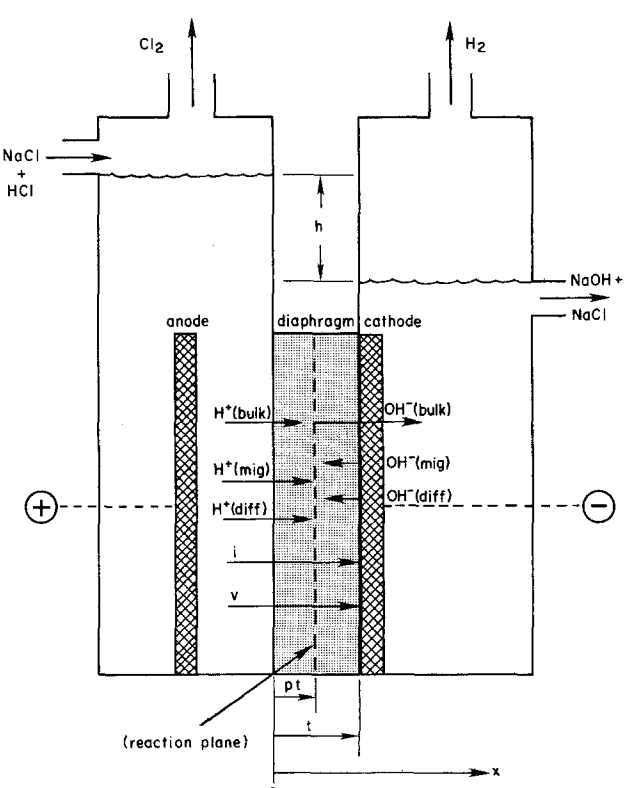

Fig. 1. Schematic of a diaphragm-type chlorine/caustic electrolyzer

*Electrochemical Society Active Member.

[1]The phrase "simple model" is used here to mean a model with a linear potential gradient through the diaphragm.

(*vi*) the percolation velocity through the diaphragm is related to the differential head, h, according to Darcy's law, with an average viscosity, μ, (12)

$$v = \frac{P}{\mu}\frac{\rho g h}{t} \qquad [5]$$

where ρ is the density of the anolyte; (*vii*) the diaphragm is divided into two regions by a reaction plane located at position pt (see Fig. 1) such that H^+ ions are present only on the anolyte side of the reaction plane and OH^- ions are present only on the catholyte side of the reaction plane; at the plane, the acid-base reaction (reaction [2]) occurs in such a manner that the concentrations of both H^+ and OH^- ions are equal to the square root of the inverse of their equilibrium constant; (*viii*) water vapor loss from the catholyte is negligible, so that the hydroxyl ion concentration at the diaphragm/catholyte interface equals the hydroxyl ion concentration in the electrolyzer effluent; (*ix*) water vapor loss from the anolyte and homogeneous reactions of hydrogen ion with dissolved chlorine are negligible, so that the hydrogen ion concentration in the brine feed equals the hydrogen ion concentration at the anolyte/diaphragm interface; alternatively, one could consider the anolyte pH as an independent variable.

It is perhaps worth mentioning here that Eq. 6.4-7 of Bird, Stewart, and Lightfoot (13) could be used for the superficial velocity instead of Darcy's equation. Choosing to do so would introduce a need to know the porosity and specific surface area of the diaphragm instead of the permeability, P. Since P can be calculated directly from flow *vs.* head data, whereas the specific surface area and porosity cannot be determined easily, the permeability is easier to use and, consequently, preferable to the porosity and specific surface area as a means of characterizing the fluid flow through the diaphragm (see MacMullin (14) and Greenkorn (15) for additional discussion).

With the above assumptions, the steady-state material balance equations for hydroxyl ion on the catholyte side of the reaction plane (*i.e.*, for $pt \le x \le t$) and for hydrogen ion on the anolyte side of the reaction plane (*i.e.*, $0 \le x \le pt$) can be written as

$$\frac{dN_i}{dx} = 0 \qquad [6]$$

where $i = 1, 2$ for OH^-, H^+, respectively.

The flux expression for both species in the porous diaphragm can be written (11) as follows

$$N_i = -\frac{D_i}{N_M}\frac{dC_i}{dx} - \frac{z_i D_i \mathbf{F}}{N_M RT} C_i \frac{d\Phi}{dx} + vC_i \qquad [7]$$

Substituting Eq. [4] and [5] into Eq. [7] yields

$$N_i = \frac{-D_i}{N_M}\frac{dC_i}{dx} + \left(\frac{z_i D_i \mathbf{F} i}{RT\kappa} + \frac{P\rho g h}{\mu t}\right) C_i \qquad [8]$$

Defining a dimensionless distance

$$\xi = \frac{x}{t} \qquad [9]$$

and substituting Eq. [8] and [9] into Eq. [6] yields the governing differential equation for species i

$$\frac{d^2C_i}{d\xi^2} - A_i\frac{dC_i}{d\xi} = 0 \qquad [10]$$

where

$$A_i = \left(\frac{z_i \mathbf{F} i N_M t}{RT\kappa} + \frac{\rho g h P N_M}{\mu D_i}\right) \qquad [11]$$

Equation [10] applies for H^+ ion only in the interval $0 \le \xi \le p$, and for OH^- ion only in the interval $p \le \xi \le 1$, where the position of the reaction plane, p, is an unknown that must be determined as described below.

The boundary conditions for the H^+ ion are

$$\text{at} \quad \xi = 0 \qquad C_2(0) = C_{2,f} \qquad [12]$$

and

$$\text{at} \quad \xi = p \qquad C_2(p) = C_1(p) = E \qquad [13]$$

where E is the square root of the equilibrium constant for reaction [2] at the cell temperature. The boundary conditions for the OH^- ion are

$$\text{at} \quad \xi = p \qquad C_1(p) = C_2(p) = E \qquad [14]$$

and

$$\text{at} \quad \xi = 1 \qquad N_1(t) = vC_1(t) - i/\mathbf{F} \qquad [15]$$

where $N_1(t)$ is Eq. [8] evaluated at $x = t$ (*i.e.*, $\xi = 1$) and v is given by Eq. [5].

After integration of Eq. [10] and application of the boundary conditions [12] and [13], the concentration of H^+ ions can be written in terms of the reaction plane position

for $0 \le \xi \le p$

$$C_2(\xi) = C_{2,f} - (C_{2,f} - E)\left[\frac{\exp(A_2\xi) - 1}{\exp(A_2 p) - 1}\right] \qquad [16]$$

and for $p \le \xi \le 1$

$$C_2(\xi) = E \qquad [17]$$

Similarly, the concentration profile for OH^- ions can be obtained from integration of Eq. [10] with the boundary conditions [14] and [15] in terms of the reaction plane position, p

for $0 \le \xi \le p$

$$C_1(\xi) = E \qquad [18]$$

and for $p \le \xi \le 1$

$$C_1(\xi) = E + G[\exp(A_1\xi) - \exp(A_1 p)] \qquad [19]$$

where

$$G = \frac{\dfrac{\mathbf{F} i E N_M t}{RT\kappa} - \dfrac{i N_M t}{D_1 \mathbf{F}}}{\dfrac{\mathbf{F} i N_M t}{RT\kappa}\exp(A_1 p) - \dfrac{\rho g h P N_M}{\mu D_1}\exp(A_1)} \qquad [20]$$

The dimensionless reaction plane position, p, is determined from the condition that, at the plane, the flux of H^+ is equal to but in the opposite direction of OH^-

$$N_1(pt) + N_2(pt) = 0 \qquad [21]$$

Since $C_1(p) = C_2(p)$ according to assumption (*vii*), Eq. [21] can be written as

$$\delta \left.\frac{dC_1}{d\xi}\right|_{\xi=p} + \left.\frac{dC_2}{d\xi}\right|_{\xi=p} = (\delta A_1 + A_2)E \qquad [22]$$

where A_i is given by Eq. [11] and

$$\delta = \frac{D_1}{D_2} \qquad [23]$$

Equations [16] and [19] can be used in Eq. [22] to obtain

$$\delta A_1 G[\exp(A_2 p) - 1]\exp(A_1 p) - A_2(C_{2,f} - E)\exp(A_2 p) - E(\delta A_1 + A_2)[\exp(A_2 p) - 1] = 0 \qquad [24]$$

Equation [24] can be solved for p (by Newton's method, for example) after the operating parameters ($C_{2,f}$, i, h, and T) and diaphragm properties (N_M, t, and P) and the physical constants (D_1, D_2, κ, E, μ, and ρ) have been specified. Substitution of this value of p into Eq. [16] and [19] then yields explicit expressions for the concentration profiles for H^+ and OH^- ions. Also, once the value of p has been determined, the effluent caustic concentration, $C_1(\xi = 1)$, can be predicted according to Eq. [19] with $\xi = 1$

$$C_1(1) = E + G[\exp(A_1) - \exp(A_1 p)] \quad [25]$$

Equation [25] can be used to obtain an expression for the caustic yield, η, (often referred to as the caustic current efficiency) according to the following definition

$$\eta = \frac{vC_1(1)\mathbf{F}}{i} \quad [26]$$

Substitution of Eq. [25] and [5] into Eq. [26] yields

$$\eta = \frac{E\mathbf{F}\rho ghP}{i\mu t} + \frac{\left[\frac{E\mathbf{F}\rho ghP}{i\mu t} - \frac{RT\kappa\rho ghP}{D_1\mathbf{F}i\mu t}\right]\left\{\exp[A_1(1-p)] - 1\right\}}{1 - \frac{RT\kappa\rho ghP}{D_1\mathbf{F}i\mu t}\exp[A_1(1-p)]} \quad [27]$$

where

$$A_1 = \frac{-\mathbf{F}iN_M t}{RT\kappa} + \frac{\rho ghPN_M}{\mu D_1} \quad [28]$$

Equations [27] and [28] show that, for this model, the important diaphragm characterizing properties for η are the product of P and N_M, the ratio of P to t, and the product of N_M and t. Note, however, that $C_1(1)$ depends only on PN_M and $N_M t$ (see Eq. [25])

Dimensionless Groups

Before proceeding to predictions of the model, it is instructive to recast some of the above equations in terms of the dimensionless groups presented earlier (4). That is, Eq. [27] can be rewritten as follows

$$\eta = \frac{E}{C_F N_H} + \frac{\left[\frac{E}{C_F N_H} + \frac{\mathrm{Pe}}{\Delta\phi}\right]\{\exp[A_1(1-p)] - 1\}}{1 + \frac{\mathrm{Pe}}{\Delta\phi}\exp[A_1(1-p)]} \quad [29]$$

where Pe is the Peclet number and is written here in terms of the differential head

$$\mathrm{Pe} = \frac{\rho ghPN_M}{\mu D_1} \quad [30]$$

$-\Delta\phi$ is the dimensionless voltage drop

$$-\Delta\phi = -\frac{\mathbf{F}}{RT}[\Phi(\xi=1) - \Phi(\xi=0)] = \frac{\mathbf{F}iN_M t}{RT\kappa} \quad [31]$$

and N_H is the Hine number

$$N_H = \frac{i}{C_F v\mathbf{F}} \quad [32]$$

Also A_1 and A_2 can be written in terms of these dimensionless groups

$$A_1 = \Delta\phi + \mathrm{Pe} \quad [33]$$

and

$$A_2 = -\Delta\phi + \mathrm{Pe}\delta \quad [34]$$

The Peclet number is a measure of the effect of convection relative to diffusion and is used routinely by chemical engineers. The dimensionless voltage drop, $-\Delta\phi$, can be thought of as the importance of the effect of ionic migration. The Hine number, N_H, is a measure of the electrochemical reaction rate relative to convection through the diaphragm; N_H should be referred to as the Hine number, since Hine and Yasuda (16) were apparently the first to recognize the significance of $i/v\mathbf{F}$.

These dimensionless groups can also be used to write an expression for the dimensionless concentration distribution of OH^- ions within the diaphragm

$$\psi_1(\xi) = \frac{C_1(\xi)}{C_F} = \frac{E}{C_F} + \frac{\left[\frac{E}{C_F} + \frac{\mathrm{Pe}N_H}{\Delta\phi}\right]\{\exp[A_1(\xi - p)] - 1\}}{1 + \frac{\mathrm{Pe}}{\Delta\phi}\exp[A(1-p)]} \quad [35]$$

Similarly, these dimensionless groups can be substituted into Eq. [20] and into Eq. [24] to show that the plane position and, hence, the dimensionless hydroxyl ion concentration depend upon six and seven dimensionless groups, respectively; that is

$$p = f_p\left(-\Delta\phi, \mathrm{Pe}, N_H, \delta, \frac{C_{2,f}}{C_F}, \frac{E}{C_F}\right) \quad [36]$$

and

$$\psi_1(\xi) = f_1\left(-\Delta\phi, \mathrm{Pe}, N_H, \delta, \frac{C_{2,f}}{C_F}, \frac{E}{C_F}, \xi\right) \quad [37]$$

Also, the caustic yield and the dimensionless H^+ concentration depend, respectively, on the same six and seven dimensionless groups. In addition, it is interesting to note that when the hydrogen ion concentration in the anolyte, $C_{2,f}$, is equal to the equilibrium concentration, E, the reaction plane position is at the anolyte/diaphragm interface (*i.e.*, Eq. [24] is satisfied trivially with $p = 0$). When $C_{2,f} = E$, $\psi_1(\xi)$ depends only on ξ and three dimensionless groups ($-\Delta\phi$, Pe, and N_H), and when $p = 0$ and $E = 0$, the caustic yield, (Eq. [29]), depends on only two dimensionless groups ($-\Delta\phi$, and Pe), as shown previously (4, 5).

Model Predictions

The reaction plane position and the concentration distributions of H^+ and OH^- ions within the diaphragm can be obtained once values have been set for the operating variables (T, $C_{2,f}$, i, and h), the diaphragm properties (N_M, t, and P), and the physical constants (D_1, D_2, κ, ρ, μ, and K_{eq}). Table I presents the values used for the parameters and identifies i, h, and $C_{2,f}$ (for Fig. 3) as the variable independent operating variables.

Figure 2 presents the concentration distributions predicted by the model for the case where i is fixed at approximately 0.0926 A/cm² and the differential head varies. Note that the predicted concentration distributions for H^+ and OH^- approach each other and drop rapidly to 10^{-10} mol/cm³ at the reaction plane. The reason for this is the large equilibrium constant for reaction [2] ($K_{eq} \cong 10^{20}$ cm⁶/mol²). In other physical systems, the reaction plane approximation (Eq. [21] and assumption (*vii*)) may not be valid because the reaction zone may not be thin enough to be considered a plane. In such cases, an alternative formulation of the problem that is based on the method used by Hsueh and Newman (17) can be used (12).

Table I. Parameter values for model predictions shown in Fig. 2-9

Fixed Independent Operating Variables
- T = 358.15 K
- $C_{2,f}$ = 3.0×10^{-5} mol/cm³ (except for Fig. 3)

Variable Independent Operating Variables
- i, h

Fixed Independent Diaphragm Properties
- N_M = 2.0
- t = 1.0 cm
- P = 5.80×10^{-11} cm²

Fixed Physical Constants
- D_1 = 3.50×10^{-5} cm²/s
- D_2 = 1.51×10^{-4} cm²/s
- κ = 0.50 Ω^{-1} cm^{-1}
- ρ = 1.17 g/cm³
- μ = 1.10×10^{-2} g/cm-s
- E[a] = $(K_{eq}^{-1})^{0.5} = (C_1C_2)^{0.5} = 10^{-10}$ mol/cm³

[a] K_{eq} is assumed here to be a constant equal to 10^{20} cm⁶/mol² for convenience.

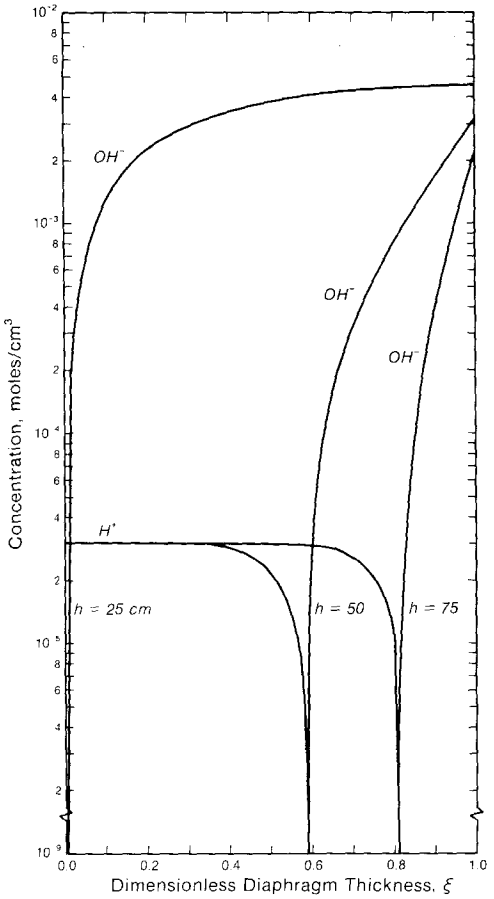

Fig. 2. Dependence of the concentration profiles on h at i = 0.0926 A/cm².

Figures 3 and 4 show the dependence of the reaction plane position on the three operating variables: h, $C_{2,f}$, and i. As shown in Fig. 3, the reaction plane moves toward the catholyte when the head is increased at a fixed anolyte pH and current density, as expected. Similarly, at a fixed head, the plane moves toward the catholyte as the anolyte pH is decreased (Fig. 3) or as the current density is decreased (Fig. 4).

Figure 5 shows that at small differential head values the caustic yield is very sensitive to the head and becomes even more so at lower current densities. However, for relatively large values of h, the predicted caustic yield is relatively insensitive to h, especially for the largest current density. It is interesting to note that the strong sensitivity of η to head changes, as shown in Fig. 5, may not be solely a function of the reaction plane position. This seems reasonable because the breakthrough (*i.e.*, rapid change in plane position) in Fig. 4 appears to be equally sensitive to head changes for all current densities. It may be then that the increased sensitivity of η is a result of η being a combination of independent (*i.e.*, i and h) and dependent (*i.e.*, $C_1(1)$ and p) variables.

Figure 6 shows that the caustic effluent concentration is sensitive to h except for i = 0.154 A/cm² over the range of 0-50 cm. Comparison of Fig. 4 and 6 for i = 0.154 A/cm² reveals that the insensitivity of the effluent concentration

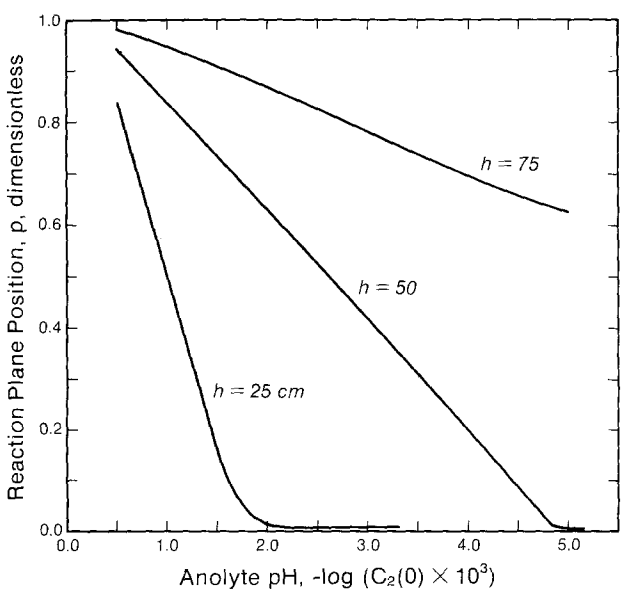

Fig. 3. Dependence of the reaction plane position on h and $C_{2,f}$ (anolyte pH) at i = 0.054 A/cm².

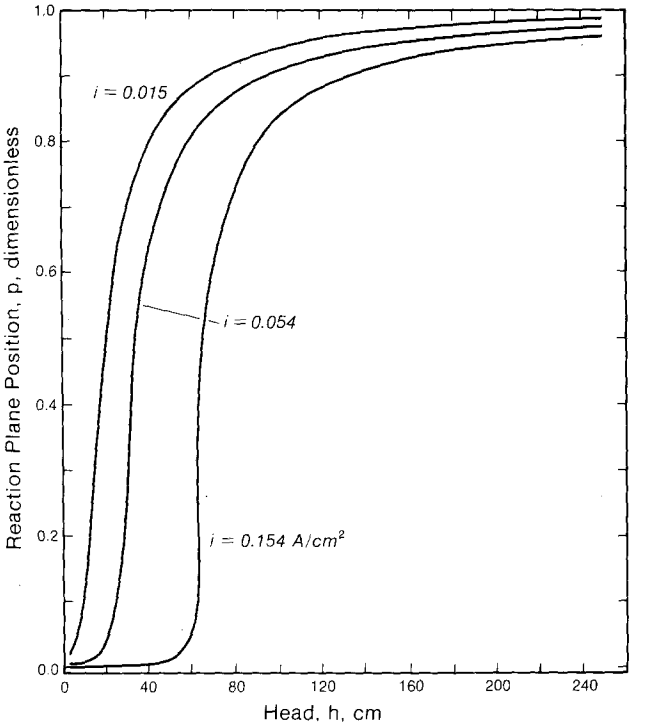

Fig. 4. Dependence of reaction plane position on current density and head.

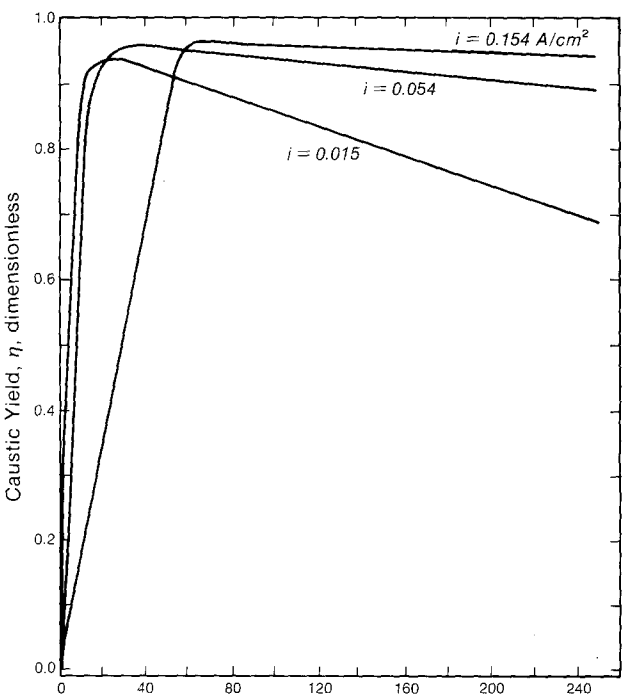

Fig. 5. Effect of head and current density on caustic yield

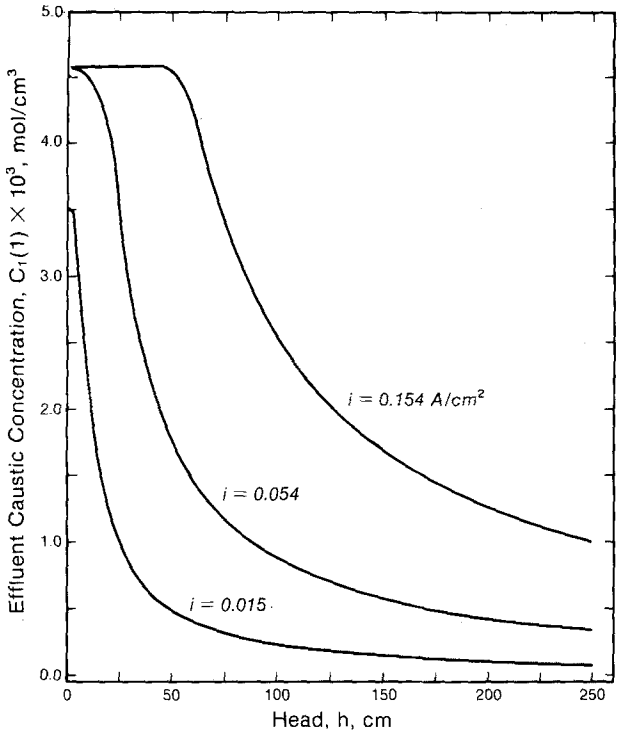

Fig. 6. Effect of head and current density on effluent caustic concentration.

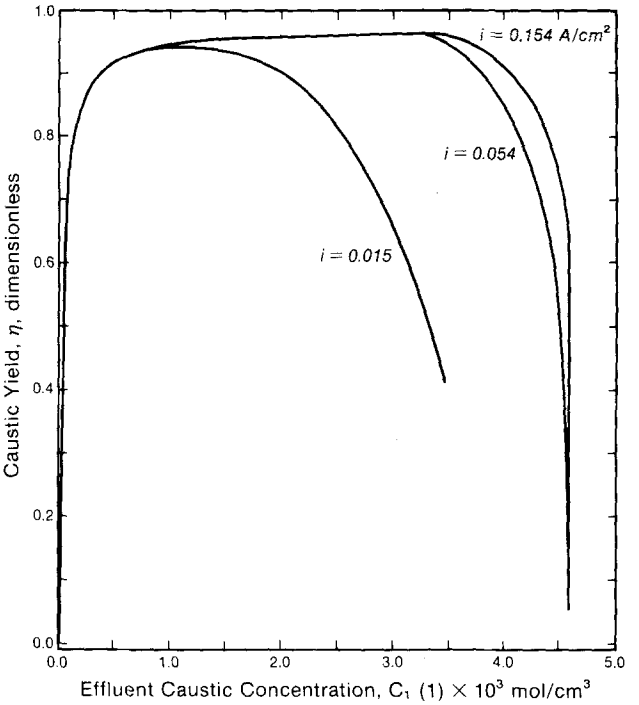

Fig. 8. Effect of current density on the dependence of caustic yield on caustic effluent concentration.

to head changes between 0-50 cm is due to the reaction plane being at the anolyte/diaphragm interface.

Figures 7 and 8 show how η depends on the reaction plane position, p, and the effluent caustic concentration, $C_1(1)$, at various current densities. Figure 7 shows that η can be large (>0.9), even though the diaphragm is in some cases almost 90% full of H^+ ions (*i.e.*, $p = 0.9$). Figure 8 shows that the caustic yield decreases at both low and high caustic effluent concentrations. This decrease in η at low effluent concentrations has been observed experimentally (18) and has been predicted by a more complicated diaphragm model (11), but it cannot be predicted by simple models in which the reaction plane position is fixed at the anolyte/diaphragm interface. That is, a predicted maximum in the relationship of caustic yield and effluent concentration is due to the acid-base reaction plane within the diaphragm.

Figure 9 shows the difference between the predicted caustic yields from a model (4, 5) that fixes the plane position at the anolyte/diaphragm interface (*i.e.*, $p = 0$) and the model presented here at an anolyte pH of about 1.5. The difference decreases as the current density increases, but, at a current density of 0.054 A/cm^2, a 3-4% difference in the predicted η values between the two models would be expected for a head of 40 cm.

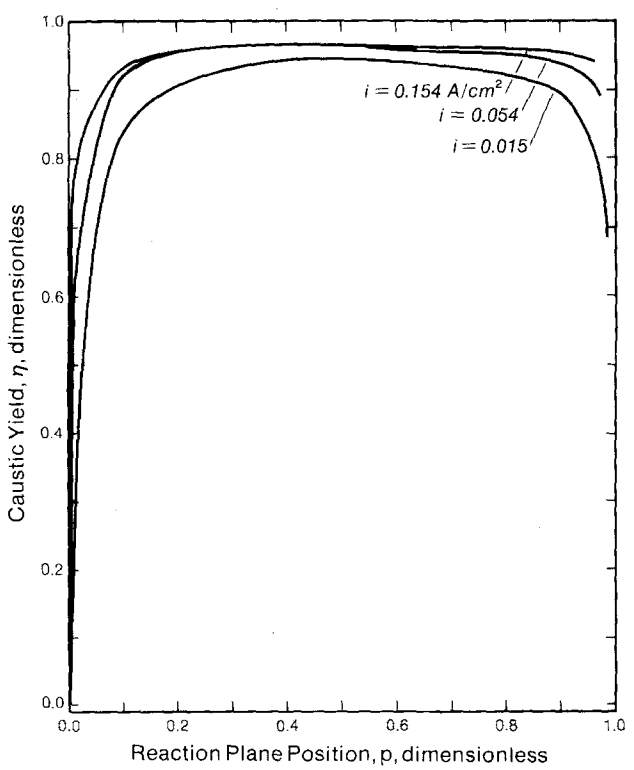

Fig. 7. Effect of current density on the dependence of caustic yield on reaction plane position.

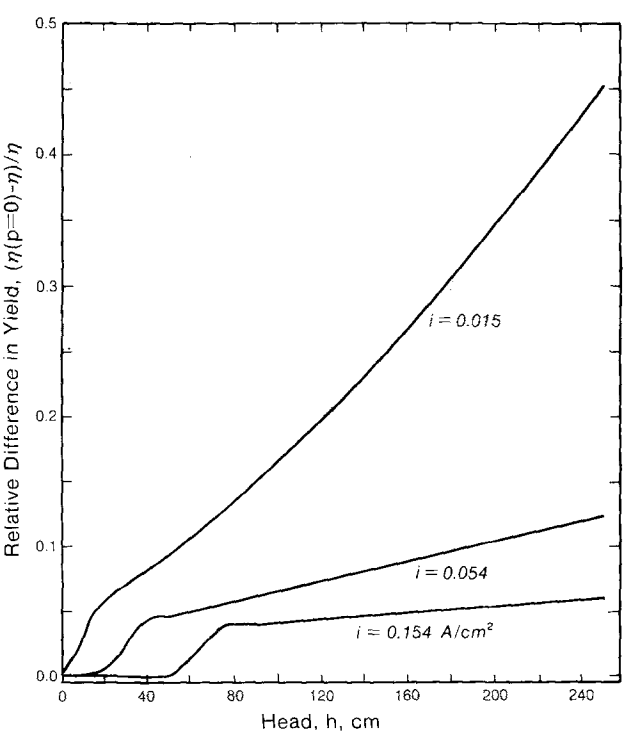

Fig. 9. Effect of head and current density on relative difference between a model with p fixed at $\xi = 0$ and the model presented here.

Comparison to Experimental Data

In this section, the reaction plane model presented above is compared with the data of Ref. (3) and with a model (4, 5) in which the plane position is fixed at the anolyte/diaphragm interface. In order to make these comparisons, the velocity through the diaphragm was used instead of the head as an independent variable. This replacement is accomplished by using Eq. [5] to obtain an explicit expression for h in terms of v, P, ρg, μ, and t and then by substituting this expression into Eq. [25] and [27]. This is necessary because the velocity rather than the head was set in the experiments (3) and because the fixed plane model (4, 5) was developed with the velocity through the diaphragm as an independent variable.

The diaphragm model presented above can be compared with the data of Ref. (3) once values of the physical constants of the model are specified. These values could be obtained from the literature, if available, or they could be determined from separate experiments. Alternatively, the physical constants could be estimated by nonlinear least squares (LS) regression of Eq. [25] or [27] against measured values of a dependent variable ($C_1(\xi = 1)$ in Eq. [25]) or a variable derived from a combination of dependent and independent variables (η, in Eq. [27]). With this regression approach, the model is "fitted" to the data, and statistical theory (19-23) is used to state that the parameter estimates are the best values for the data in the sense that the estimates result in a minimum difference between the observed and predicted values of, for example, η. Then, the model with these estimates can be used for interpolation within the data set. Confidence is gained in the mechanistic or theoretical model if the parameter estimates obtained by LS are physically realistic, and extrapolation beyond the range of the data may be made with caution within the limits of the assumptions of the model. Also, if the number of data points is large, confidence intervals for the parameter estimates can be obtained in the same manner as in linear regression (21, 22).

The estimation of D_1, D_2 and κ by LS requires experimental data in which N_M, t, and $C_{2,f}$ are known quantities. The factorially designed experiments of Ref. (3) provided data in which N_M was varied from 3.3 to 7.5, t was varied from 0.17 to 0.33 cm, and $C_{2,f}$ was varied from about 1×10^{-5} to $8 \times 10^{-2}M$. Again, the velocity was substituted for the head as an independent variable so that the current density and velocity were set as independent variables. Also, the temperature was controlled at 70° ± 0.5°C, and the NaCl concentration of the brine feed was held constant at 5.13M over all of the experiments. The diaphragm voltage drop and the concentration of OH^- ion in the effluent were measured simultaneously as dependent variables.

The details of the LS regression procedure are described in the Appendix. The LS estimates of the pertinent transport parameters are shown in Table II. The large confidence interval for D_2 shown in Case A of Table II probably indicates that the acid concentrations in the experiment were not large enough for accurate estimation of D_2. That is, even though the model predicts reaction plane positions within the diaphragm ($0.1 \leq p \leq 0.6$) for 18 of the data points with the parameters of Case A (12), these data are not sufficient to determine D_2 with confidence. This is not a fault of the model, nor of the experimental data, but, rather, it is an indication that an experiment designed for the specific purpose of estimating D_2 is needed. This point is further illustrated by the parameters of Case B of Table II, which were determined by fixing the plane position at the anolyte/diaphragm interface (5). Comparison of Case A and Case B values for D_1 and κ shows that either model (*i.e.*, the variable plane model or the fixed plane model) could be used to estimate these parameters with confidence from the data of Ref. (3). Also the estimates of $\hat{\sigma}_1^2$ for both cases are about equal, and they yield an average difference between the observed and predicted values of η of about 3% (*i.e.*, average difference = $(\eta^0 - \eta) = (1.110 \times 10^{-3})^{1/2} \times 100$). This average difference indicates a relatively good fit for either model, especially since the error of titration required to measure η is about 2%.

Table II. Parameter estimates for reaction plane diaphragm model

Parameter	Estimate	±	95% Confidence interval	Units
Case A. Parameter estimates with variable plane position: $\hat{\sigma}_1^2 = 1.119 \times 10^{-3}$, $\hat{\sigma}_2^2 = 2.688 \times 10^{-3}$ V², $N = 84$, $M = 64$.				
D_1	2.810×10^{-5}	±	0.114×10^{-5}	cm²/s
D_2	3.339×10^{-5}	±	4.842×10^{-5}	cm²/s
κ	0.337	±	0.016	Ω^{-1} cm^{-1}
$G(\beta)$	1.611×10^{2}		—	none
Case B. Parameter estimates with plane position fixed at $x = 0$(5): $\hat{\sigma}_1^2 = 1.118 \times 10^{-3}$, $\hat{\sigma}_2^2 = 2.688 \times 10^{-3}$ V², $N = 84$, $M = 64$.				
D_1	2.826×10^{-5}	±	0.112×10^{-5}	cm²/s
κ	0.338	±	0.016	Ω^{-1} cm^{-1}
$G(\beta)$	1.627×10^{-2}		—	none

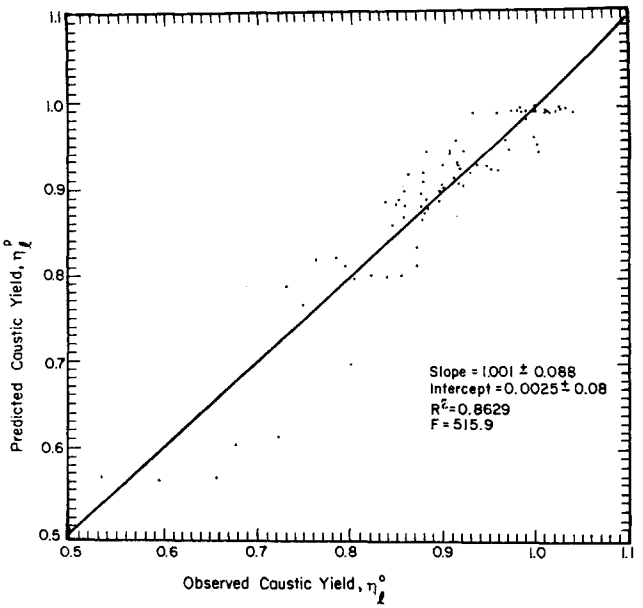

Fig. 10. Comparison of model predictions and experimental caustic yield data.

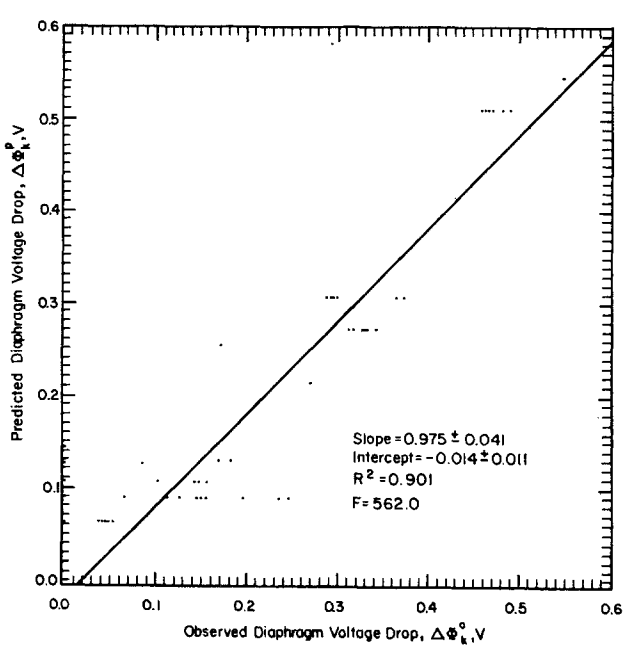

Fig. 11. Comparison of model predictions and experimental diaphragm voltage drop data.

Figures 10 and 11 show a comparison of the predicted and observed caustic yields and diaphragm voltage drops for the data of Ref. (3) and the parameter estimates of Case A. The residuals (*i.e.*, the difference between the predicted and observed values) are independent of the dependent variables (12) as required by LS regression theory (19, 20). Also, plots of the residuals and of the independent variables (12) indicate no correlation between these variables and the residuals. Thus, it can be concluded that the model with the LS estimates of Case A of Table II can be used to predict both the caustic yield and the diaphragm voltage drop when the anolyte is either acidic or neutral, when the velocity through the diaphragm is specified.

Conclusions

Formulation of a simple model that accounts for the acid-base neutralization reaction within the diaphragm in terms of measurable diaphragm properties has provided a design equation that allows direct comparison of experimental and theoretical predictions. This comparison, accomplished with parameter estimation techniques, shows that the predicted values for the caustic yield and voltage drop through the diaphragm are reasonable; changing the assumption of a linear potential gradient through the diaphragm may provide an improvement. Analysis of the parameter estimates showed that an additional designed experiment is needed in order to estimate with confidence the diffusion coefficient of hydrogen ion.

Acknowledgment

The authors acknowledge gratefully that this work was supported in part by Dow Chemical USA.

APPENDIX

Nonlinear Regression Procedure

Since the predictions of the caustic yield and the diaphragm voltage drop are coupled through the average conductivity, κ, an appropriate LS objective function is

$$G(\underline{\beta}) = \sum_{l=1}^{N} \frac{(\eta_l^{\circ} - \eta_l)^2}{\hat{\sigma}_1^{\,2}} + \sum_{k=1}^{M} \frac{(\Delta\Phi_k^{\circ} - \Delta\Phi_k)^2}{\hat{\sigma}_2^{\,2}} \quad [A\text{-}1]$$

where β is the vector of parameters, $[D_1 D_2 \kappa]^T$, η_l is predicted by Eq. [27] (modified to use v instead of h as described above) at the experimental conditions corresponding to the l^{th} datum, $\Delta\Phi_k$ is predicted by integration of Eq. [4] at the experimental conditions corresponding to the k^{th} datum, and $\hat{\sigma}_1^{\,2}$ and $\hat{\sigma}_2^{\,2}$ represent the estimated variance of η and $\Delta\Phi$, respectively, as discussed below. The nonlinearity of Eq. [A-1] results from the nonlinear model equation for η, but it does not affect the use of the theory behind LS regression (22, 23). The computations necessary to minimize the above objective function become more complicated with a nonlinear function, but many computers have subroutine libraries that can perform the necessary calculations. In this work, minimization subroutines of the International Mathematical and Statistical Library (24) were used (12).

Each of the estimated variances ($\hat{\sigma}_1^{\,2}$ and $\hat{\sigma}_2^{\,2}$) in Eq. [A-1] corresponds to the sum of the variance associated with the measurement error and the variance associated with the model error. That is, we assume (in accordance with the assumptions of LS theory) that any difference between the observed and predicted values is a lumped error that is distributed randomly. Thus, $\hat{\sigma}_1^{\,2}$, for example, was calculated by dividing the minimum value of $G(\underline{\beta})$ when $\hat{\sigma}_2^{\,2} = \infty$ by the degrees of freedom (in this case, $N - 3$, since three parameters are adjusted to minimize $G(\underline{\beta})$). Similarly, $\hat{\sigma}_2^{\,2}$ was calculated by dividing the minimum value of $G(\underline{\beta})$ when $\hat{\sigma}_1^{\,2} = \infty$ by $M - 1$ (only one parameter, κ, is adjusted to minimize $G(\underline{\beta})$ when $\hat{\sigma}_1^{\,2} = \infty$). The weighting of the dependent variables in this fashion gives the "best values" (23) of the parameters for Eq. [27] and [4] and the data. These estimated variances and parameters are shown in Case A of Table II.

LIST OF SYMBOLS

A_i dimensionless driving force for species i, see Eq. [11]
C_i, $C_i(x)$, $C_i(\xi)$ concentration of species i at position x or ξ, mol/cm³
$C_{2,f}$ H^+ ion feed concentration, mol/cm³
C_F NaCl feed concentration, a constant reference quantity, mol/cm³
D_i free-stream diffusion coefficient of species i, cm²/s
$D_{i,e}$ effective diffusion coefficient of species i, cm²/s
E equilibrium concentration of OH^- and H^+ ions, *e.g.*, 10^{-10} mol/cm³ at 298 K; *i.e.*, $E = (K_{eq}^{-1})^{0.5}$
$\mathbf{F}$ Faraday's constant, 96,487 C/mol of electrons
G see Eq. [20], mol/cm³
$G(\underline{\beta})$ least squares objective function, see Eq. [A-1], dimensionless
g acceleration due to gravity, cm/s²
h differential head, cm
i current density, A/cm²
K_{eq} equilibrium constant for reaction [2], cm⁶/mol²
M number of data points for voltage drop data
N number of data points for caustic yield data
N_M MacMullin number, see Eq. [3], dimensionless
$N_i(x)$, N_i flux of species i at position x, mol/cm²-s
N_H Hine number, see Eq. [32], dimensionless
P Darcy's law permeability, cm²
Pe Peclet number, see Eq. [30], dimensionless
p reaction plane position, dimensionless
R gas constant, 8.3143 J/mol-K
T temperature, K
t diaphragm thickness, cm
v superficial percolation velocity through the diaphragm, cm/s
x diaphragm dimensional coordinate, cm
z_i ionic charge of species i, $z_1 = -1$ and $z_2 = 1$, dimensionless

Greek

β vector of parameters, $[D_1 D_2 \kappa]^T$, for example
δ ratio of free-stream diffusion coefficients, dimensionless
ϵ porosity, dimensionless
η caustic yield or caustic current efficiency, see Eq. [26], dimensionless
η_l° observed caustic yield, dimensionless
κ average solution conductivity, Ω^{-1} cm^{-1}
μ average solution viscosity, g/cm-s
Φ, $\Delta\Phi$ dimensional voltage, voltage drop through the diaphragm, V
$\Delta\Phi_k^{\circ}$ observed voltage drop through diaphragm, V
$-\Delta\phi$ dimensionless voltage drop through the diaphragm, see Eq. [31]
$\psi_1(\xi)$ dimensionless concentration of OH^-, see Eq. [35]
ρ anolyte solution density, g/cm³
$\hat{\sigma}_1^{\,2}$, $\hat{\sigma}_2^{\,2}$ estimated variance of caustic yield and diaphragm voltage drop, dimensionless and V², respectively
τ tortuosity of diaphragm, dimensionless
ξ dimensionless diaphragm coordinate, see Eq. [9]

REFERENCES

1. D. L. Caldwell, in "Comprehensive Treatise of Electrochemistry," Vol. 2, J. O'M. Bockris, B. E. Conway, E. Yeager, and R. E. White, Editors, pp. 121-129, Plenum Press, New York (1981).
2. J. Van Zee, R. E. White, and A. T. Watson, *This Journal*, **133**, 501 (1986).
3. K. A. Poush, D. L. Caldwell, J. W. Van Zee, and R. E. White, in "Modern Chlor-Alkali Technology," Vol. 2, C. Jackson, Editor, pp. 21-36, Ellis Horwood Limited, Chichester, West Sussex, England (1983).
4. R. E. White, J. S. Beckerdite, and J. Van Zee, in "Electrochemical Cell Design," R. E. White, Editor, pp. 25-60, Plenum Press, New York (1984).
5. J. Van Zee and R. E. White, *This Journal*, **132**, 818 (1985).
6. T. Mukaibo, *J. Electrochem. Soc. Jpn.*, **20**, 482 (1952).
7. T. K. Sherwood, R. L. Pigford, and C. R. Wilke, "Mass Transfer," Chap. 8, McGraw-Hill, New York (1975).
8. R. White, J. Trainham, J. Newman, and T. W. Chapman, *This Journal*, **124**, 669 (1977).
9. R. E. White, Ph.D. dissertation, University of California, Berkeley, CA (1977).
10. J. S. Newman, "Electrochemical Systems," p. 217, Prentice-Hall, Inc., Englewood Cliffs, NJ (1973).
11. D. L. Caldwell, K. A. Poush, J. W. Van Zee, and R. E. White, in "Electrochemical Processes and Plant Design," R. C. Alkire, T. R. Beck, and R. D. Varjian, Editors, The Electrochemical Society Softbound Proceedings Series, Pennington, NJ (1983).
12. J. W. Van Zee, Ph.D. Dissertation, Texas A&M University, College Station, TX (1984).

13. R. B. Bird, W. E. Stewart, and E. L. Lightfoot, "Transport Phenomena," pp. 196-200, John Wiley & Sons, Inc., New York (1960).
14. R. B. MacMullin and G. A. Muccini, *J. AIChE.*, **2**, 393 (1956).
15. R. A. Greenkorn, "Flow Phenomena in Porous Media," Chap. 3, Marcel Dekker, Inc., New York (1983).
16. F. Hine and Y. Yasuda, *This Journal*, **118**, 116 (1971).
17. L. Hsueh and J. Newman, *Ind. Eng. Chem., Fundam.*, **10**, 615 (1971).
18. V. L. Kubasov, V. B. Vorobeva, and L. I. Yurkov, *Sov. Electrochem.*, **15**, 1773 (1979).
19. R. J. Freund and P. D. Minton, "Regression Methods," p. 25, Marcel Dekker Inc., New York (1979).
20. B. Ostle and R. W. Mensing, "Statistics in Research," 3rd ed., pp. 166-178, Iowa State University Press, Ames, IA (1975).
21. A. R. Gallant, *Am. Stat.*, **29**, 73 (1975).
22. A. R. Gallant and D. W. Jorgenson, *J. Econometrics*, **11**, 275 (1979).
23. N. Draper and H. Smith, "Applied Regression Analysis," 2nd ed., pp. 108-112, John Wiley & Sons, Inc., New York (1981).
24. International Mathematics and Statistical Library subroutine ZXSSQ, IMSL, Houston, TX.

Electrochemical and Spectral Investigations of Oxidative Pathways of 6-Chloro-2,3,4,5-Tetrahydro-1-(4-Hydroxyphenyl)-1*H*-3-Benzazepine-7,8-Diol

Fenoldopam

Hung-Yuan Cheng, Louisa Lam Davis,* R. Lee Webb, Steven Carr, Gerald D. Roberts, David B. Staiger, and Gary E. Zuber

Department of Analytical, Physical, and Structural Chemistry, Smith Kline and French Laboratories, Philadelphia, Pennsylvania 19101

ABSTRACT

Fenoldopam, a selective D-1 dopamine receptor agonist currently under development for treatment of hypertension and congestive heart failure, undergoes two-electron, two-proton oxidation in acidic to neutral pH aqueous buffer to form the corresponding *o*-quinone, **8**. The fate of **8** in aqueous solution depends on *p*H, with a half-life of a few seconds at *p*H 7.4 to a few days in 0.1*M* HCl. Certain physiologically important nucleophiles and reducing agents also react rapidly with **8**. For example, **8** is reduced immediately by ascorbic acid to **1**. In the presence of glutathione (GSH), both the 6 and 9 positions of **8** can be attacked by the sulfhydryl nucleophile to form 6-Cl-9-SG and 6,9-di-SG adducts. Spectral studies show that substitutions at the 6 and 9 positions induce a systematic change in the infrared region. Additionally, circular dichroism (CD) spectra indicate that the configuration of the chiral center for the R- or S-enantiomer is preserved in these reactions. Oxidation of the 8-*O*-sulfate of **1**, an important metabolite of **1** in mammals, is at a much more positive potential. However, the unstable oxidation product is rapidly hydrolyzed to form **8**. The biological implications, as well as synthetic and analytical utilities, of these findings are discussed.

In the development of chemical treatments for cardiovascular diseases, significant effort has been devoted to searching for compounds with high specificities toward peripheral dopamine receptors (1,2). Compound **1**, 6-chloro-2,3,4,5-tetrahydro-1-(4-hydroxyphenyl)-1*H*-3-benzazepine-7,8-diol (fenoldopam; SK&F 82526), is a potent D-1 receptor agonist which possesses selective peripheral dopamine agonist activities (3-5). The enantioselectivity and dopaminergic activities of **1** and several structurally related benzazepine compounds have been investigated and compared with various receptor models derived from studies on other classes of dopamine agonists and antagonists (6,7). Currently, this compound is under clinical trials for treatment of hypertension and congestive heart failure (8).

The biological significance of redox interactions has been a subject of considerable interest in dopamine research (9-14). In recent years, electrochemical studies of such agonists and antagonists as dopamine (15-18), apomorphine (19), and chlorpromazine (20-22) have provided viable chemical models for the postulated links between their redox chemistry and *in vitro* dopaminergic activities. While it has not been established that electron transfer processes are directly related to *in vivo* functionalities, it is generally agreed that many of the oxidative reactions have physiological implications. The objectives of this study are as follows. First, fenoldopam oxidizes at approximately the same potential as dopamine, but shows different reaction patterns following the initial oxidation. We would like to gain a detailed understanding of the oxidative pathways of fenoldopam so that we can compare the redox behavior of this selective D-1 receptor agonist with other dopamine receptor agonists. Second, the ease of oxidation for fenoldopam in buffers near neutral *p*H suggests that under certain circumstances oxidative degradations of this compound might occur in biological systems. We would like to identify and characterize some of the reaction products in aqueous solution under a controlled oxidative environment. Third, the heterogeneous electrochemical process is known to offer certain advantages over the homogeneous chemical approach in organic synthesis (23), and therefore we are interested in determining the feasibility of using this process in small scale synthesis of pharmacologically active compounds. Here, we place our focus on oxidative coupling of physiologically significant nucleophiles to the dihydroxyphenyl backbone (24). Many of such reactions and products have been hypothesized to have biological significances (15, 16, 19).

Three new benzazepine derivatives, **9-11**, were isolated and identified in this study. A number of existing benzazepine compounds (**2-7, 12**) structurally related to **1** were used for comparative studies. These are compounds which have different substitutions at the 6 or 9 position on the 7,8-dihydroxyphenyl ring, or at the 4′ position on the 1-phenyl ring.

Experimental

Apparatus.—Cyclic voltammetry was carried out with either an EG&G Princeton Applied Research Model 174A potentiostat or a Bioanalytical Systems Model 100 Analyzer. All peak potentials reported are *vs.* a saturated

* Electrochemical Society Active Member.